Article

The International Journal of
Robotics Research
2015, Vol. 34(13) 1559–1572

DOI: 10.1177/0278364915585397
ijr.sagepub.com

Hand-held transendoscopic robotic manipulators: A transurethral laser prostate surgery case study

Richard J. Hendrick[1], Christopher R. Mitchell[2], S. Duke Herrell[2] and Robert J. Webster III[1]

Abstract

Natural orifice endoscopic surgery can enable incisionless approaches, but a major challenge is the lack of small and dexterous instrumentation. Surgical robots have the potential to meet this need yet often disrupt the clinical workflow. Hand-held robots that combine thin manipulators and endoscopes have the potential to address this by integrating seamlessly into the clinical workflow and enhancing dexterity. As a case study illustrating the potential of this approach, we describe a hand-held robotic system that passes two concentric tube manipulators through a 5 mm port in a rigid endoscope for transurethral laser prostate surgery. This system is intended to catalyze the use of a clinically superior, yet rarely attempted, procedure for benign prostatic hyperplasia. This paper describes system design and experiments to evaluate the surgeon's functional workspace and accuracy using the robot. Phantom and cadaver experiments demonstrate successful completion of the target procedure via prostate lobe resection.

Keywords

Surgical robotics, medical robotics, concentric tube robots, prostate surgery, HoLEP, benign prostatic hyperplasia

1. Introduction

Endoscopic surgery enables access to surgical sites through small incisions and has become the standard of care for many types of surgeries. In recent years, there has been increasing interest in further reducing invasiveness by eliminating skin incisions completely, in favor of delivering endoscopes and manipulators through natural orifices. A major challenge in natural orifice surgeries is maintaining the dexterity of both the endoscope and surgical instruments in the presence of the constraints imposed by the natural orifice and anatomical pathway to the surgical site. Because of this, natural orifice procedures are typically difficult to complete when first conceived of by forward-thinking surgeons, because procedure-specific instrumentation has yet to be developed.

The surgical robotics community has been actively engaged in remedying this in recent years by developing small manipulators which can be passed through (or alongside) endoscopes, to provide surgeons with enhanced dexterity and larger workspaces. There has been a great deal of interest in particular in single port surgeries, where the robot enters the body through a small incision, typically in the abdomen.

For example, the system design of Piccigallo et al. (2010) delivered two six-degree-of-freedom (DOF) manipulators, with motors embedded in the manipulator arms, through a 30 mm umbilical access port. Lehman et al. (2011) focused on triangulation with an elbow-based design that delivered two four-DOF arms, one for cautery and one equipped with a gripper, for dissection tasks through a 26 mm abdominal port. Phee et al. (2008) demonstrated a 24 mm system which could be delivered via the mouth or anus with an endoscope and two six-DOF manipulators driven by Bowden cables for scarless gastrointestinal surgery. The 19 mm ViaCath system was introduced in Abbott et al. (2007), and delivers two six-DOF flexible, nylon manipulators and a standard flexible endoscope through the mouth

[1]Vanderbilt Department of Mechanical Engineering, Vanderbilt University, Nashville, TN, USA
[2]Vanderbilt Department of Urologic Surgery, Vanderbilt University, Nashville, TN, USA

Corresponding author:
Richard J. Hendrick, Vanderbilt Department of Mechanical Engineering, Vanderbilt University, VU Station B 351592, 2301 Vanderbilt Place, Nashville, TN 37235-1592, USA.
Email: richard.j.hendrick@vanderbilt.edu

to access the gastrointestinal tract. The compact design of Shang et al. (2012) delivered two articulated arms with interchangeable instruments and an articulated camera through a 16 mm port. The single-port design with perhaps the smallest diameter to date that delivers two manipulators was shown by Ding et al. (2013). Their flexible robotic platform provides two seven-DOF continuum manipulators and a three-DOF stereo vision module via a single 15 mm incision. The above are just a few of the many examples of the surgical robotics community's active and ongoing efforts to increase the dexterity, visualization capability, and workspace of surgeons in single port and natural orifice settings.

These systems demonstrate the remarkable progress that has been made in the design and miniaturization of robotic surgical systems, but some of the most demanding natural orifice applications (e.g. nostril, ear canal, or transurethral procedures) require further miniaturization. Another challenge in the clinical adoption of many robotic systems is that they often significantly affect the clinical workflow, for example by moving the surgeon from direct interaction at the patient's bedside to a console away from the patient. Indeed, it has been suggested that future surgical robotic systems should devote increasing attention to clinical workflow by including features such as smaller, more ergonomic actuation units (see e.g. Taylor and Stoianovici, 2003), with compact functionality (see e.g. Camarillo et al., 2004), and hands-on surgeon interfaces (see e.g. Rodriguez y Baena and Davies, 2010).

In keeping with these ideas, in this paper we present a hand-held system that fits seamlessly into the current clinical workflow for transurethral laser-based treatment of benign prostatic hyperplasia (BPH). Our objective in creating this robot is to catalyze the use of a procedure that is known to be clinically superior, yet is rarely attempted by surgeons because of the degree of difficulty associated with accomplishing it with current instruments. This procedure is holmium laser enucleation of the prostate (HoLEP) wherein the surgeon uses a laser fiber introduced through a straight, rigid endoscope to manually resect prostate tissue (see Figure 1). The robotic system we have developed gives surgeons manual, hand-held control of both the endoscope and two concentric tube robotic manipulators that pass through the 5 mm port included in the endoscope (see Figure 2).

Concentric tube robots are a type of miniature, needle-sized continuum robot composed of concentric, precurved, elastic tubes first proposed for use as robotic manipulators simultaneously by Webster III et al. (2006) and Sears and Dupont (2006). They are typically made of superelastic nitinol, which is well suited for this application because it has large recoverable strain and can be shape-set into desired curves while maintaining its superelasticity. When these precurved tubes are translated and rotated at their bases, their elastic interaction creates "tentacle-like" motion (elongation and bending) of the device.

Geometrically exact mechanics-based models now exist for these manipulators (Dupont et al., 2010; Rucker et al., 2010) and a variety of real-time control methods have been described (Burgner et al., 2014; Dupont et al., 2010; Xu and Patel, 2012).

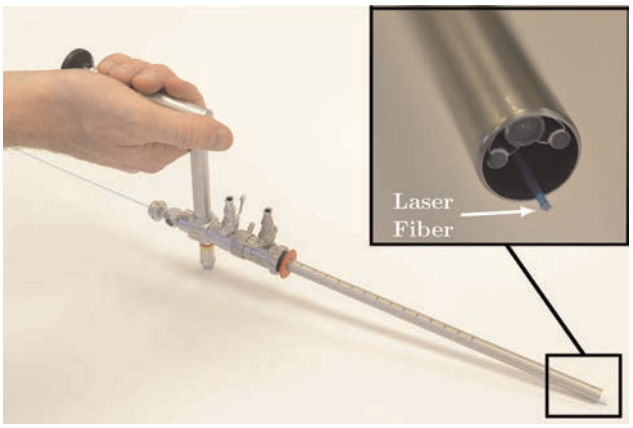

Fig. 1. An image of a transurethral endoscope (Storz, Inc. 27292 AMA) with a HoLEP laser fiber introduced through the working channel. In a HoLEP procedure, the surgeon grasps a similar endoscope outside the patient, passes it transurethrally to the prostate, and manually adjusts endoscope pose to attempt to simultaneously control endoscope view, bring the laser to bear on the desired target, and manipulate soft tissue with the endoscope tip. The challenge of accomplishing all three tasks simultaneously is generally agreed to be the reason HoLEP can currently only be offered by a few of the most skilled physicians, despite proven clinical benefits for the patient.

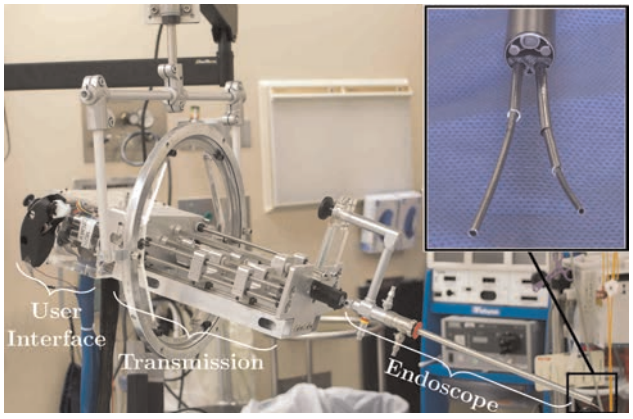

Fig. 2. Our new robotic system integrates two concentric tube manipulators with a standard clinical endoscope in a hand-held (counterbalanced) system. The system fits seamlessly into the clinical workflow because the surgeon still has direct manual control of endoscope pose, and can simultaneously control the manipulators that extend through the endoscope with thumb and finger motions.

Concentric tube robots are particularly well suited to the hand-held paradigm due to the small size and weight of the manipulators and the fact that actuators can be located away from the surgical site, at tube bases. The hand-held approach in surgical robotic devices has been previously

beneficially applied in the context of articulated laparoscopic forceps (Yamashita et al., 2004), hand-held da Vinci tools (Focacci et al., 2007), steerable needles (Okazawa et al., 2005), and articulated endoscopic tools (Shang et al., 2011), among others. For concentric tube robots, a single-tube robot has been employed as a reach extender in eye surgery (Wei et al., 2009) and in neuroendoscopy to deliver an electrocautery wire (Butler et al., 2012). Our robot follows the hand-held paradigm of these prior systems, but is the first system of which we are aware that has incorporated multiple concentric tube manipulators in a hand-held device.

As briefly mentioned earlier, our system is clinically motivated by the prospect of increasing the utilization of HoLEP to treat BPH, a procedure that has demonstrated excellent clinical outcomes, yet is rarely used because of its degree of difficulty for the surgeon. HoLEP is currently conducted using a straight, rigid endoscope, which the surgeon holds and introduces transurethrally into the prostate. A straight holmium laser fiber is passed through the working channel of the endoscope and used to resect (i.e cut, not thermally ablate) the tissue. The holmium laser is a "contact laser" intended to be positioned in close proximity to the target tissue to be cut. Beneficial aspects of the laser in this surgical procedure are its ability to both cut and cauterize tissue simultaneously and the fact that thermal energy is highly localized (Mandeville et al., 2011). Enucleation refers to the use of the laser to resect the prostate tissue as a solid mass ("peeling" internal prostate tissue away from the prostate capsule without cutting into it). Once the mass of tissue is free, it is then pushed into the bladder. A device called a morcellator is then introduced through the urethra into the bladder and used to simultaneously cut the prostate tissue into small pieces and remove it from the body using suction.

HoLEP has been clinically demonstrated to have significantly better outcomes for patients than traditional transurethral resection of the prostate (TURP) procedures, which use sharp dissection or electrocautery. The benefits include a 50% reduction in catheterization time, a 33% reduction in hospitalization duration, and the elimination of the need for blood transfusions (Ahyai et al., 2007). Recently, long-term follow-up data has shown that HoLEP requires fewer re-operations, which is leading many in the urology community to conclude that HoLEP should become the new gold standard treatment for enlarged prostate (Van Rij and Gilling, 2012). Despite these compelling clinical advantages, HoLEP is currently conducted at only a few institutions because it is extremely challenging for the surgeon (Lingeman, 2011). It is physically demanding because large forces are required to angle the endoscope, due to the soft tissues surrounding it. To make matters worse, the surgeon must simultaneously manipulate soft tissue using the endoscope itself, and bring the laser fiber (which has no articulation, aiming straight out from the endoscope at a fixed position with respect to the image) to bear on the desired surgical target, which requires a high degree of surgical skill. The robotic system described in this paper is designed to make HoLEP easier by providing two independent concentric tube manipulators, introduced through the existing working channel of a standard clinical endoscope. These two concentric tube manipulators can be used cooperatively by the surgeon: one arm facilitates tissue manipulation and retraction, while the other aims the laser fiber.

The transurethral approach in our system draws inspiration from several prior robotic systems. TURP was one of the earliest surgical robotics applications (Davies, 2006; Davies et al., 1991) in which a robotized endoscope was used for autonomous sharp dissection of the prostate, based on medical imaging. Somewhat surprisingly, since this pioneering work, only a few research groups have developed robotic systems designed for transurethral deployment. In 2001, robotic transurethral laser resection of the prostate through a standard endoscope was briefly mentioned (Ho et al., 2001), though the authors' main focus was on the Nd:YAG laser used, rather than on the robotic system. In 2002, master–slave teleoperation of a robot holding an endoscope for TURP was described (De Badajoz et al., 1998). In 2004, a four-DOF manipulator for prostate resection delivering a drill and cutter through an 8 mm rigid tube, with ultrasound guidance, was developed (Hashimoto et al., 2004). Here, a major focus was on the removal of excised tissue from the body, since a morcellator was not available. In 2013, the feasibility of transurethral robotic bladder access was demonstrated by Goldman and colleagues, which was the first use of a continuum robot in a transurethral application. This robot consisted of a 5 mm continuum manipulator that delivered a laser fiber, a fiberscope, and biopsy forceps into the bladder for visual inspection and tumor resection (Goldman et al., 2013). Our system follows the continuum robot paradigm of Goldman et al., but focuses on the prostate rather than the bladder. It also differs in the use of the continuum robots as manipulators at the tip of the endoscope rather than as an outer deflectable tube for carrying instruments to the surgical site.

1.1. Contributions

The primary contribution of this paper is to establish the feasibility of single-operator hand-held control of an endoscope and two articulated transendoscopic manipulators. Within the prostate surgery application, the system we describe is the first hand-held robot for transurethral surgery of which the authors are aware, and also the first robotic system specifically designed to facilitate the HoLEP procedure. A design contribution is the idea of using field-of-view reachability as an objective function for optimally selecting tube parameters in a concentric tube robot. Experimental contributions include a comparison of task space control and joint space control that demonstrated the surgeons were more accurate using task space control, contrary to the experimenting surgeons' initial assumption that joint space control would be superior, and a

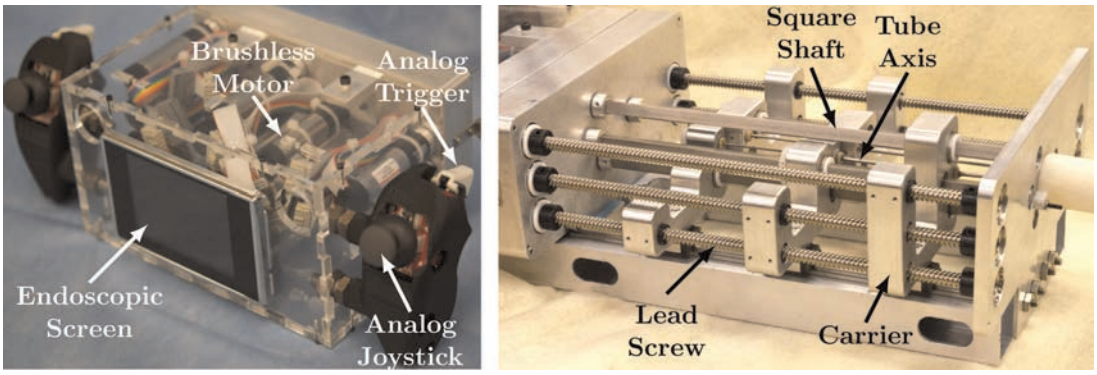

Fig. 3. (Left) The user interface section houses the motors and has two handles which are equipped with joysticks and triggers that give the surgeon control of each manipulator, while a screen displays the endoscopic view. (Right) The transmission section: square shafts transmit torque to rotate the concentric tubes, and lead screws drive tube carriers to translate the tubes.

demonstration of the system's practicality via phantom and cadaver HoLEP resection experiments.

This paper is an archival unification of results previously described in preliminary form at three conferences (Hendrick et al., 2014a,b,c). In addition to merging and streamlining results from these three sources, noteworthy additions/enhancements in the current paper include a more detailed analysis and discussion of benchtop experimental results including reporting additional experimental data, as well as the first report of a cadaver experiment with the system.

2. System design

There are two elements to the design of our system: the mechanical design of the actuation unit and user interface, and the selection of tube curvatures in the manipulators. The overall system consists of four main modules: the user interface (Figure 3, left), the transmission (Figure 3, right), the endoscope (Figure 5, left), and the counterbalance (Figure 5, right).

2.1. Mechanical design

At the end of the robot nearest the surgeon is the user interface module (see Figures 2 and 3, left). This module is designed to quick-connect to the transmission module through spring-loaded shaft couplings and houses nine 16 mm, 8 W brushless motors with 29:1 gearheads (Maxon Motor, Inc.). Fixed to the outside of the user interface module are handles, where the surgeon grasps the robot and can manually manipulate the entire system to control endoscope pose. Each handle has an embedded joystick and trigger that are used to control the concentric tube manipulators. A screen is also placed between the surgeon's hands, which can be used to display the endoscopic view.

The transmission section (see Figures 2 and 3, right) converts the rotation of the motors in the user interface module into translation and rotation of the tubes. The

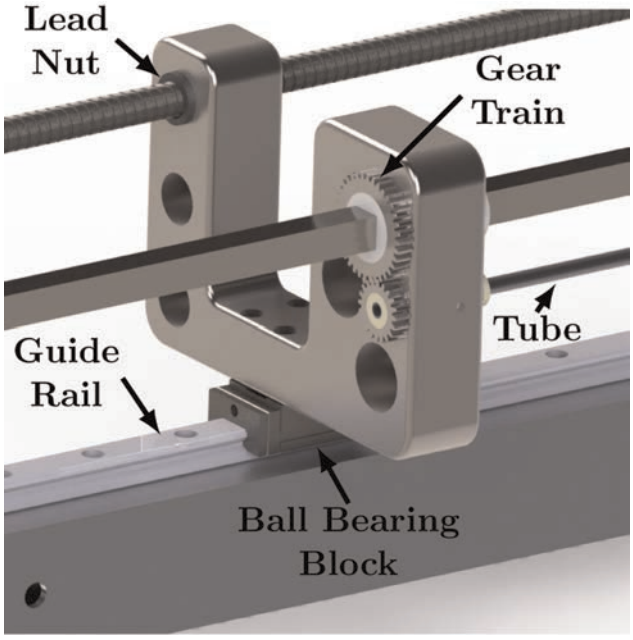

Fig. 4. A detailed view of a single carrier is shown. Rotation of the square shaft transmits torque through the gear train and rotates the tube. Rotation of the lead screw translates the carrier on the guide rail which translates the tube.

transmission was designed such that one concentric tube manipulator could include three precurved tubes (six DOF), while the other manipulator could include two tubes with the outer tube straight (three DOF). In the set of experiments described in this paper, however, both arms were configured as two-tube, three-DOF manipulators. Linear motion of the tubes is achieved via lead screws ($0.33\ ^{\text{in}}/_{\text{rev}}$), which drive tube carriers that ride on ball bearing blocks on a guide rail. Rotation of the tubes is achieved via square shafts, which transmit torque through a gear train to the tube; see Figure 4 for a detailed view of a single carrier. By using square shafts that run the entire length of the transmission section, torque can be transmitted

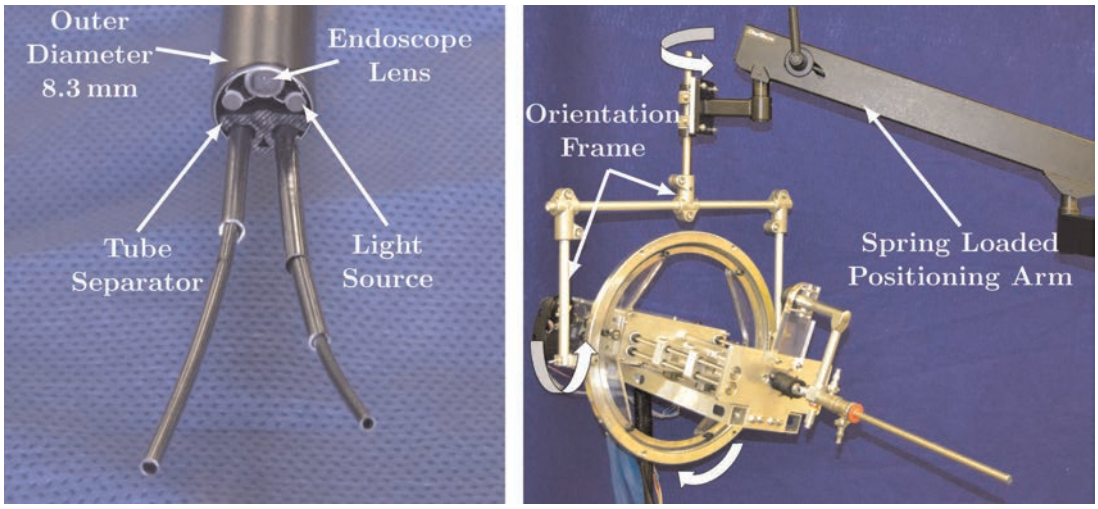

Fig. 5. (Left) The rigid endoscope is shown with two concentric tube robots passing through it. The endoscope and two fiber optic bundles providing illumination are built into the endoscope. The two manipulators pass through a single 5 mm port inside the endoscope. A custom plastic tube separator constrains the exit axes of each manipulator at the endoscope tip. (Right) A spring-loaded positioning arm provides passive gravity compensation and a custom orientation frame provides orientation DOF for the surgeon.

over a variable distance, allowing the motors to be static and compactly packaged. Friction was mitigated throughout the transmission section by choosing plastic (PET) lead nuts, a ball bearing block that rides on the guide rail, and a PTFE sleeve that translates on the square shaft. Friction between the interacting tubes also affects the system. The effect is minimal in translation, since the axial stiffness of the tubes make it easy to break static friction. In rotation, however, the tubes can store torsion such that the tube rotation at its base is not equal to the tube rotation at the tip. To mitigate this effect, adequate clearance between the tubes is critical.

The endoscope (see Figures 2 and 5, left) is mounted to the front of the transmission section and is a clinical 26 Fr (8.28 mm) endoscope (Storz, Inc. 27292 AMA). Because this endoscope is rigidly mounted to the robot, manipulation of the robot via the user interface handles also manipulates the endoscope. This endoscope contains optics and light sources as well as a 5 mm tool channel, through which we pass our concentric tube robots. A 500 μm laser fiber is passed through the inner channel of one of the robotic arms. Because the manipulators and the endoscope lens have a fixed geometric relationship independent of endoscope pose, the transformations between the user interface, endoscope, and manipulator frames are all constant.

To assist the surgeon by supporting the weight of the hand-held robot, a spring-loaded counterbalanced arm (Dectron, USA) is provided (Figure 5, right). A custom orientation frame was also constructed, providing three passive orientation DOF so that the overall counterbalance system enables the surgeon to manipulate the robot freely in six DOF without perceiving the system as having any weight. When the robot is used in transurethral prostate surgery, the endoscope approximately operates through an anatomically constrained center of motion near the front of the prostate. This constraint is created by the soft tissue pressure provided by the urogenital diaphragm. Thus, the surgeon must typically manually coordinate four-DOF endoscope motion (roll, pitch, yaw, and insertion) during surgery.

2.2. Tube design: Optimizing the reachable field of view

Design optimization of concentric tube robots is an active area of research. Tube parameters can be optimized to maximize the reachability of a target anatomical volume (Burgner et al., 2013), or to navigate through constrained anatomy and reach specified target positions (Bedell et al., 2011). In HoLEP, since the endoscope view and manipulator bases will move together and be repositioned during surgery, it is desirable for the manipulators to be able to reach as much of the endoscope's field of view as possible. Thus, to design optimal manipulators for HoLEP, we maximize the overlap between the endoscopic field of view and the workspace of the manipulator (i.e. the "reachable field of view" (RFOV)). To determine the RFOV, we must model both the endoscope's field of view and the concentric tube robot's workspace, and then compute the intersection of the two.

We model the field of view of the endoscope as a cone with its vertex at the lens. Manufacturer specifications describe this endoscope as having a 6° angle of view, 103° field of view, and 30 mm depth of view, and we determined that the lens is located approximately 1.2 mm from the tip of the endoscope. The modeled field of view is shown in Figure 7. In considering manipulator workspace, we note that while it is possible to use several tubes and non-constant precurvatures, in this paper we restrict our attention to manipulators consisting of a straight outer tube and a constant curvature inner tube. These tubes can move

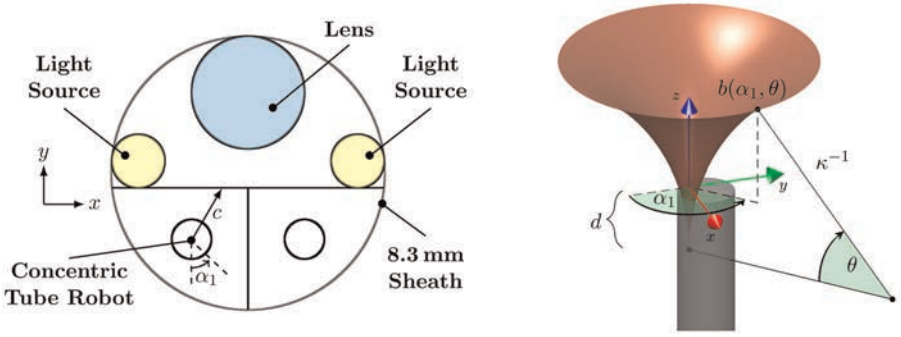

Fig. 6. (Left) A cross-section of the endoscope tip. The concentric tube manipulator base frame is located a short distance inside the tip of the endoscope, and its workspace is partially defined by the boundary indicated in black straight lines in the figure above. The boundary is defined by the endoscope sheath, a line tangent to the light sources, and the midline of the endoscope between the two manipulators. (Right) The workspace surface, $b(\alpha_1,\theta)$, of a concentric tube robot is shown. The chosen coordinate frame and all parameters required to calculate the surface are illustrated for an example point on the surface.

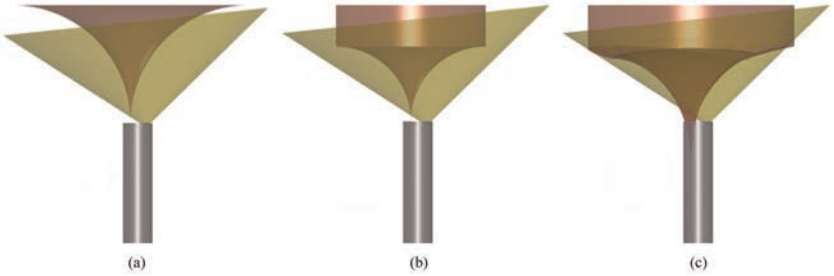

Fig. 7. Manipulator workspace overlaid on field of view for (a) a tube design of κ = 30.1 m^{-1} (RFOV=8.9%), (b) optimal design with manipulator base at endoscope tip (κ = 47.8 m^{-1}, RFOV=29.5%), and (c) optimal design (κ = 34.6 m^{-1}, RFOV=64.9%) when the manipulator base is located inside the tip of the endoscope.

in three DOF, and RFOV optimization is conducted over one parameter, namely the curvature (κ) of the inner tube. The concentric tube manipulator's position in the endoscope cross-section is shown in Figure 6.

In the absence of constraints, the manipulator's trumpet-shaped workspace can be analytically determined by revolving a circular arc with a cylinder appended, as shown in Figure 7. In practice, RFOV can be increased by placing the base of the concentric tube robot a short distance inside the tip of the endoscope, so that the manipulator can begin to curve before passing out of the tip of the endoscope. This modification requires pushing the tube separator from Figure 5 a short distance into the tip of the endoscope. Under these conditions the concentric tube manipulator's workspace is also limited by the boundary shown in Figure 6. Important quantities in mathematically describing this boundary on the workspace include the rotation of the inner tube (α_1), the clearance between the manipulator axis and the boundary ($c(\alpha_1)$), the radius of the inner tube (r), the angle subtended by the curved portion of the inner tube (θ), and the critical angle subtended by the inner tube at which it collides with the boundary (θ_c). This angle and the distance behind the tip of the endoscope where the straight tube should end to achieve it, d, are given by

$$\theta_c = \cos^{-1}\left(\frac{c\kappa - 1}{r\kappa - 1}\right) \tag{1}$$

$$d = \kappa^{-1}\sin(\theta_c) \tag{2}$$

From this, the trumpet-shaped workspace boundary surface, b, can be shown to be

$$b(\alpha_1, \theta) = \begin{bmatrix} -\kappa^{-1}\sin(\alpha_1)(\cos(\theta) - 1) \\ \kappa^{-1}\cos(\alpha_1)(\cos(\theta) - 1) \\ \kappa^{-1}\sin(\theta) - d \end{bmatrix} \tag{3}$$

where $\alpha_1 \in [0\ 2\pi)$, $\theta \in \left[0\ \pi/2\right]$, and an origin on the tube axis at the endoscope tip is assumed as shown in Figure 6, right. The closed curve defined at θ = 90° forms the bottom of a cylinder that extends axially to form the remainder of the workspace boundary, which can be accessed by extending out both tubes together.

We began by discretizing the curvature of the inner tube into 100 evenly spaced values within a range of 20 m^{-1} to 70 m^{-1}. The lower curvature bound was selected because it

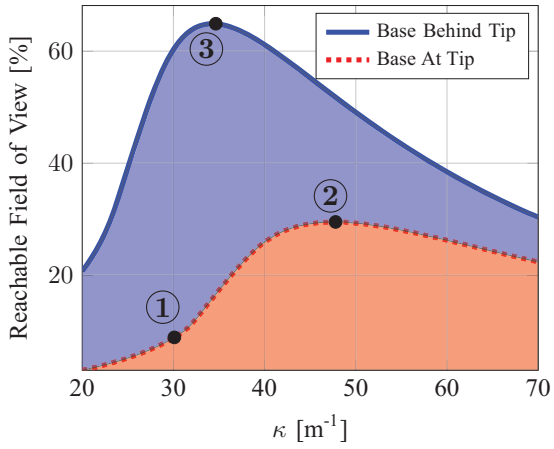

Fig. 8. RFOV as a function of tube curvature. The three labeled points correspond to the numbered illustrations in Figure 7. Base at tip refers to the base of the manipulator being at the tip of the endoscope. Base behind tip refers to the base of the manipulator being located a short distance inside the endoscope.

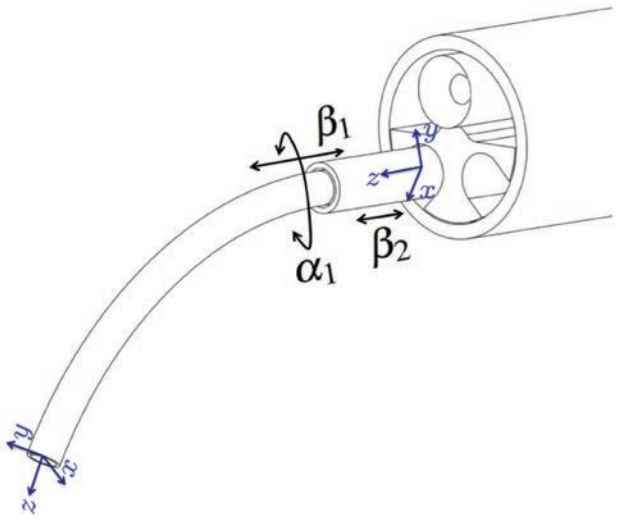

Fig. 9. The concentric tube manipulators used in our experiments are a special case where the outer tube is straight and stiff and the inner tube is curved and elastic. We define the fixed base frame of the manipulator at the tip of the endoscope, and a body-attached frame at the tip of the inner tube. Rotation of the inner tube, translation of the inner tube, and translation of the outer tube are given by the variables α_1, β_1, and β_2, respectively.

was clear geometrically that this workspace would have little overlap with the field of view, while the upper curvature bound approaches the limit of a tube that we could shape-set. We defined the radius of the inner tube as $r = 0.5$ mm to approximate our initial prototypes. For each curvature, the workspace was computed and the percentage of the visualization volume covered was determined. This was done by discretizing the visualization cone into a total of n isotropic 0.5 mm voxels and counting the n_r total voxels whose centers are inside the manipulator's workspace. This allows us to define the RFOV metric as $\text{RFOV} = {}^{n_r}/_{n}$. Three different example cases of overlaid workspace and view volume are shown in Figure 7, and RFOV versus κ is shown in Figure 8.

The most noteworthy result from this study is that locating the base of the concentric tube manipulator a short distance inside the endoscope behind its tip is useful for reaching the maximum percentage of the visualization volume, with lower required curvature.

3. Manipulator kinematics and control

This section begins by discussing the kinematics and Jacobian of the concentric tube manipulators in our handheld robotic HoLEP system. We then describe the singularity-robust resolved rates algorithm used to map surgeon inputs to manipulator tip motions.

3.1. Manipulator forward kinematics and Jacobian

The two-tube concentric tube manipulator discussed previously in the design section (Figure 9) is a special case of the general concentric tube robot model given in Rucker et al. (2010) and Dupont et al. (2010). Despite the fact that the general model must be solved numerically, this special case enables the kinematics and Jacobian of the manipulator to be written in closed form. The actuation variables are $q = [\alpha_1 \quad \beta_1 \quad \beta_2]^{\mathrm{T}}$, where α_1 denotes the angular rotation of the inner tube, $\beta_1 \in s$ (where s measures arc length) denotes the location where the inner tube is held by its carrier, and $\beta_2 \in s$ denotes the location where the outer straight tube is held by its carrier. We define $s = 0$ at the tip of the endoscope, with positive s out of the endoscope. Let ℓ_1 and ℓ_2 be the total lengths (i.e. the sum of the straight and curved lengths) of the inner and outer tubes, respectively. We define a fixed frame at the endoscope tip, with the z-axis tangent to the endoscopic axis, and its x-axis defined as the direction about which the inner tube curves at $\alpha_1 = 0$, as shown in Figure 9. We also define a body-attached frame at the tip of the robot with its z-axis tangent to the robot backbone and its x-axis in the direction about which the tube curves. Using these definitions, the forward kinematic map, g_{st}, is given by

$$g_{st} = \begin{bmatrix} R & d \\ 0 & 1 \end{bmatrix}, \quad R = \begin{bmatrix} c_{\alpha_1} & -s_{\alpha_1}c_\gamma & s_{\alpha_1}s_\gamma \\ s_{\alpha_1} & c_{\alpha_1}c_\gamma & -c_{\alpha_1}s_\gamma \\ 0 & s_\gamma & c_\gamma \end{bmatrix}$$
$$d = \begin{bmatrix} -\kappa^{-1}s_{\alpha_1}(c_\gamma - 1) \\ \kappa^{-1}c_{\alpha_1}(c_\gamma - 1) \\ l_2 + \beta_2 + \kappa^{-1}s_\gamma \end{bmatrix} \tag{4}$$

where $\gamma = \kappa(\beta_1 - \beta_2 + \ell_1 - \ell_2)$. It is shown in Murray et al. (1994) that a spatial Jacobian can be determined from the forward kinematics.

We prefer to express the velocity mapping via the hybrid Jacobian, so we convert this spatial Jacobian to a body Jacobian and then express the twists in the fixed frame, which results in the following hybrid Jacobian:

$$J_h = \begin{bmatrix} \kappa^{-1}c_{\alpha_1}(1-c_\gamma) & s_{\alpha_1}s_\gamma & -s_{\alpha_1}s_\gamma \\ \kappa^{-1}s_{\alpha_1}(1-c_\gamma) & -s_\gamma c_{\alpha_1} & s_\gamma c_{\alpha_1} \\ 0 & c_\gamma & 1-c_\gamma \\ 0 & \kappa c_{\alpha_1} & -\kappa c_{\alpha_1} \\ 0 & \kappa s_{\alpha_1} & -\kappa s_{\alpha_1} \\ 1 & 0 & 0 \end{bmatrix} \tag{5}$$

For a detailed description of this analysis in the context of constant curvature continuum robots, see Webster III and Jones (2010).

3.2. Manipulator control

A singularity exists for the concentric tube manipulator when the two tubes have their tips at the same point, which occurs when the two tubes extend the same distance out of the tip of the endoscope. To account for this singularity, we implemented a singularity-robust resolved rates algorithm based on Wampler II (1986). The update step in this algorithm is given as

$$\dot{q} = (J_h^{\mathrm{T}} J_h + \lambda^2 I)^{-1} J_h^{\mathrm{T}} \dot{x} \tag{6}$$

where

$$\lambda^2 = \begin{cases} 0, & \sigma_m \geq \varepsilon \\ \left(1 - \frac{\sigma_m 2}{\varepsilon^2}\right)\lambda_{max}^2, & \sigma_m < \varepsilon \end{cases} \tag{7}$$

Here ϵ determines how close to singularity one wishes the system to be before implementing the damping factor, λ_{max} is the maximum damping factor, and σ_m is the minimum singular value of J_h, which indicates how well-conditioned the Jacobian is (Chiaverini, 1997).

3.3. User interface mappings

The surgeon manipulates the concentric tube robots via the embedded joystick (with pushbutton capability) under his/her thumb and an analog trigger under his/her index finger. Initially, likely due to familiarity with manipulating manual clinical tools through endoscope ports, surgeons expected to prefer direct joint space control of the rotation and axial extension of the tubes. In task space control, surgeons were initially surprised by rapid robot motions near singularities, perceiving these as a lack of control of the concentric tube robot. However, this disagreed with the idea that task space teleoperation is often preferable in robotic systems. To explore this apparent contradiction, we implemented both joint and task space control in order to experimentally compare the two in user studies.

In joint space mode, the index finger trigger was mapped to rotational velocity of the inner tube ($\dot{\alpha}_1$), and upward motion of the joysticks (on each handle) were mapped to translational velocity of the tubes ($\dot{\beta}_1$, $\dot{\beta}_2$). The surgeon was able to reverse the direction of rotation by clicking the joystick and then again depressing the index finger trigger. All commanded velocities were linearly proportional to the deflection of the relevant analog input from thumb joysticks and index finger triggers. In task space mode (shown in Figure 10), the tips of the manipulators move relative to the camera frame. Thumb joystick deflections (both vertical and horizontal) were mapped to end-effector velocity commands in the plane of the endoscopic view. The index finger trigger was mapped to end effector velocity perpendicular to the image plane, and clicking the joystick reversed the direction of motion perpendicular to the image plane. In this mode, each manipulator can be independently controlled by the handle on the corresponding side of the robot, which enables bimanual operation.

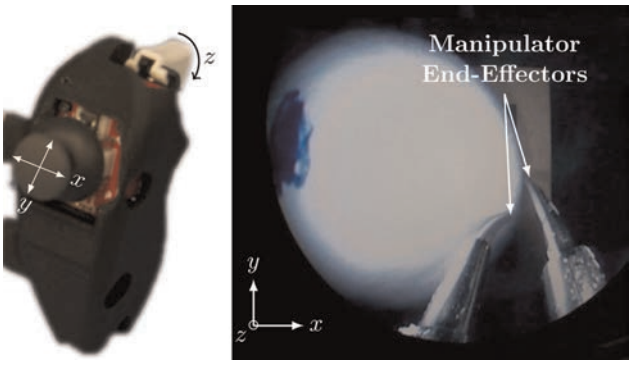

Fig. 10. (Left) One of the handles of the user interface, illustrating an analog joystick (with pushbutton) and trigger. The joystick provides for two bidirectional inputs, and the trigger gives a third unidirectional input. The pushbutton is used to reverse the direction of the trigger input. (Right) The endoscopic view is shown with the task space mapping from the user interface to the motion of the manipulator end-effectors.

4. Experiments

We evaluate the ability of surgeons to use this system to accomplish surgical objectives through four experiments described in this section. The purposes of these experiments are (1) to explore the surgeons' ability to access a larger area of relevant surgical positions with the robot compared to a standard straight endoscope, (2) to compare the surgeons' ability to follow a desired tip path using task and joint space user interface mappings, (3) to show that surgeons can use our system to perform a realistic laser resection in an anthropomorphic phantom prostate, and (4) to demonstrate a HoLEP resection procedure on an ex vivo cadaveric prostate specimen. The expert surgeons in this set of experiments are co-authors Dr Duke Herrell and Dr Christopher Mitchell.

4.1. Desired resection surface access experiment

One of the primary intended benefits of our robotic system over conventional HoLEP instrumentation is that the

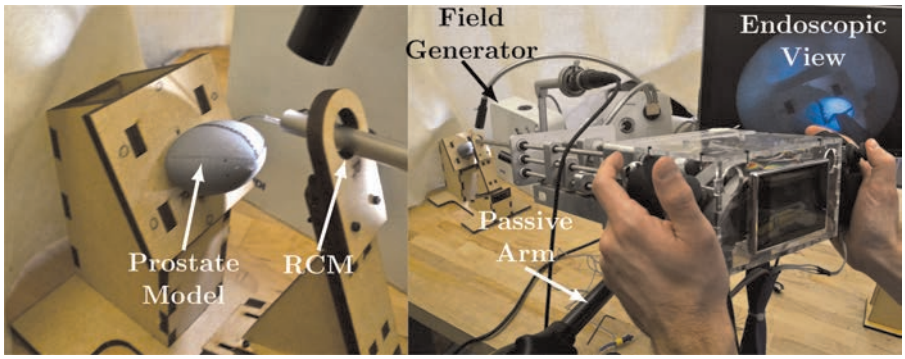

Fig. 11. The experimental setup constrains the endoscope to operate through an approximate anatomically constrained center of motion. The surgeon scans the desired resection surface (the surface of the plastic model) with the instrument tip using endoscopic video feedback. The instrument tip is magnetically tracked.

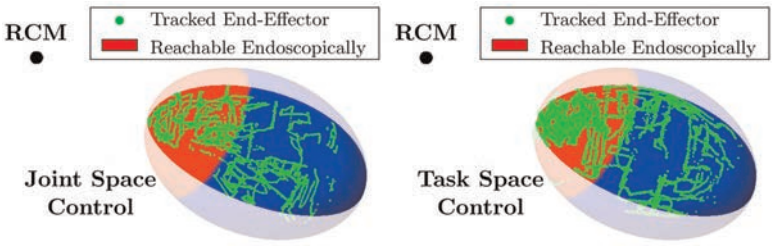

Fig. 12. Magnetic tracking data showing the positions on the desired resection surface accessed by two surgeons using the system in joint space mode (left) and task space mode (right). The lighter colored region indicates the best-case scenario for the surface reachable by a conventional straight endoscope, without tissue deformation (i.e. the reachable area without using the robot and using only a straight, rigid endoscope).

manipulators should give the surgeons easier access to resection targets, and/or access to a greater number of useful targets. In this experiment, we set out to evaluate how well the surgeon can access the intended resection surface in the prostate in a geometric sense (i.e. without tissue deformation). This test is conservative, since tissue deformation tends to help expose targets, and therefore make access easier. Disallowing deformation is a starting point in experimental validation of our system only; subsequent experiments will evaluate the ability of surgeons to use our robot for HoLEP under realistic conditions with soft tissue deformation.

To approximate the remote center of motion (RCM) imposed by the patient's soft tissues in a benchtop setting, we used a wooden support with a hole through it, positioned at an anatomically accurate distance from the prostate resection surface model. To simulate the surgeon's desired surface for laser resection in HoLEP, we affixed a 3D printed ellipsoid of anatomically correct dimensions (30 mm $\times$ 42 mm $\times$ 47 mm; Leenstra et al., 2007) made of hard plastic behind this center of motion as shown in Figure 11. A magnetic tracking system (Aurora Electromagnetic Measurement System, Northern Digital Inc.) was registered to the test stand, and a 0.5 mm electromagnetic tracking coil was embedded in the tip of the concentric tube robot.

Two experienced urologic surgeons then used the system to scan the surface of the desired resection ellipsoid. One two-tube, three-DOF manipulator was used under both joint space and task space control and the surgeons scanned one quadrant of the axially symmetric model.

This experiment was completed prior to the design of the counterbalance arm, so a passive lockable arm was used to support the robot. It was locked in place during the experiment, but the surgeons were allowed to pause surface scanning, unlock the arm and reposition the robot, and then re-lock the arm and continue scanning, as often as desired during the experiment.

The experimental results are shown in Figure 12, and a typical endoscope image during the experiment is shown in Figure 13. A cannula tip point was considered to be on the surface of the resection ellipsoid if the point was less than 2 mm from the surface in order to account for test setup registration error and magnetic tracking error. Figure 12 illustrates that surgeons were able to access nearly the entire available ellipsoidal surface of the model with both control mappings. The lighter area in Figure 12 shows the theoretical reachable area of a conventional, straight endoscope. It was computed using tangent lines to the ellipsoid that pass through the RCM. This experiment shows that our robot is capable of reaching points relevant to prostate resection. Tissue deformation is evaluated in subsequent experiments.

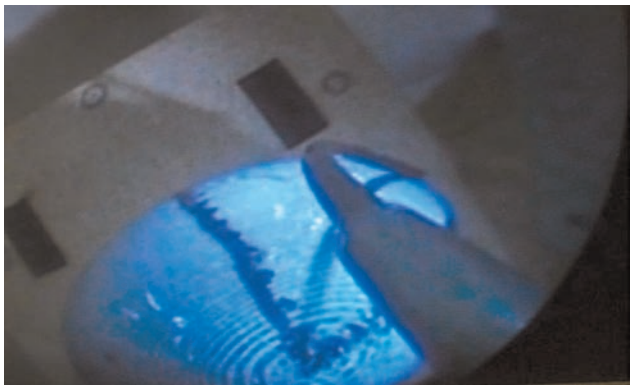

Fig. 13. Endoscopic view of a surgeon scanning the desired resection surface model.

In addition, this experiment did not reveal a difference between joint and task space operation in terms of reachability, which motivated experiments to compare them in terms of trajectory tracking, as described in the following subsection.

4.2. Trajectory tracking experiment

This experiment used the experimental setup described in the previous subsection, but rather than asking surgeons to scan the surface we asked them to follow a specified 3D curve along the surface. Both accuracy and task completion time were recorded, and surgeons were alerted to the fact that both metrics would be used for evaluation before the experiment commenced. This experiment was done once with the arm unlocked (so that the surgeons could position and orient the endoscope as well as the concentric tube manipulators to follow the path) and once with the arm locked (requiring surgeons to use only the concentric tube manipulators, without changing the endoscope pose). The paths for the two scenarios can be seen in Figure 14. These paths were drawn on the model with input from the surgeons and are intended to approximate the circumferential cuts required in a HoLEP procedure. Nevertheless, the primary aim of this experiment was to characterize the surgeon's ability to follow some desired tip path using different control modes. The ability to accomplish the entirety of a HoLEP procedure is not evaluated here, but rather in subsequent phantom and cadaver experiments presented in Sections 4.3 and 4.4.

The first path was traced with counterbalance assistance by two surgeons, each using both control modes on separate trials, each performing two trials per mode, yielding a total of eight experimental runs. The mean accuracies for both control modes with counterbalance assistance were 1.5 mm for joint space and 1.6 mm for task space. The maximum error during each run averaged 6.4 mm with joint space control and 4.3 mm with task space control. Total time to complete the task averaged 70.2 s for joint space control and 41.9 s for task space control. These results indicate that the surgeons are capable of using either control mode to follow the prescribed path, but that joint space mode required substantially more time, while also occasionally resulting in relatively large errors. Figure 15 illustrates the time surgeons spent at various levels of error.

Noting qualitatively that surgeons were using substantial endoscope manipulation, particularly with joint space control, we performed another similar experiment in which we fixed the endoscope pose by locking the counterbalanced support arm. Surgeons were then asked to trace the path shown in the center of Figure 14 using only the concentric tube manipulators. Again, two surgeons attempted to complete this task in both control modes, twice each per mode, for a total of eight experimental runs. The results of this experiment showed substantial differences for joint and task space control. First, task space control results did not change substantially from the free endoscope experiment, with a mean error of 1.6 mm and an average maximum error of 4.0 mm. The only significant difference in comparing task space control in this experiment to task space control with free endoscope movement was that surgeons traced the path more slowly. It took them approximately the same amount of time (40.3 s) to trace a shorter path in this experiment as it did to trace the longer path in the experiment with free endoscope manipulation.

The joint space control results, however, revealed a sharp contrast between free endoscope manipulation and fixed endoscope pose. Completion of the task was not achievable within a reasonable amount of time for the surgeon using joint space control with a fixed endoscope. On all four runs, the experiment was ended at surgeon request after an average time of 2 min, with over 15% of the time spent in excess of 3 mm error. We do not report the mean or maximum error since the task could not be completed, but the percentage of experiment time spent in large error states is shown in Figure 15. This indicates that the joint space control mapping was too mentally taxing for the surgeons to achieve rapidly and accurately without the assistance of endoscope pose manipulation. This means that surgeons were likely primarily using endoscope pose manipulation to trace the path in the corresponding experiment with free endoscope manipulation. This agrees with prior results where increased mental fatigue was noted with joint space operation of 3D flexible endoscopes, in which it was noted that operating these devices "quickly overwhelms the mental and motor abilities of most surgeons" (Swanstrom and Zheng, 2008).

4.3. Laser resection of an anthropomorphic prostate phantom

In this experiment, we set out to experimentally test our system in a realistic HoLEP model. We aimed to evaluate the performance of the system in an anatomically accurate model, and to explore the surgeon's ability to coordinate

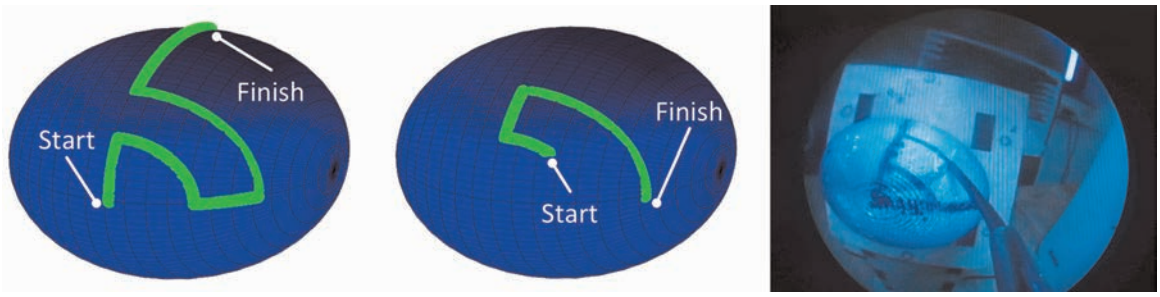

Fig. 14. (Left) Desired path of concentric tube robot tip for the experiment with free endoscope manipulation. (Middle) Desired path of concentric tube robot tip for the experiment with a fixed endoscope pose. (Right) Concentric tube robot following the desired path on the prostate resection surface model.

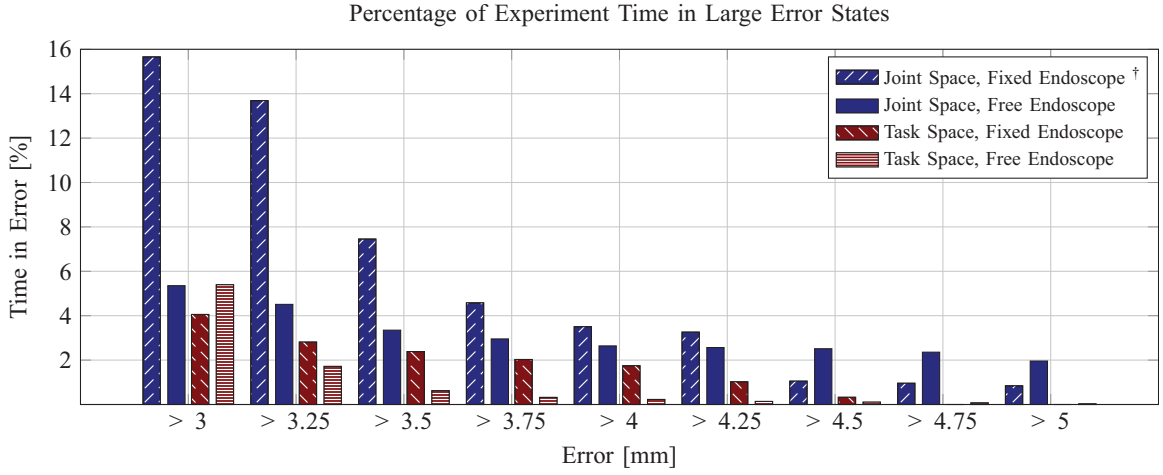

Fig. 15. An illustration of the time spent at various levels of error in the two path-tracing experiments, with and without endoscope pose manipulation. † The surgeons requested termination of this experiment prior to completion.

two concentric tube manipulators simultaneously (one to expose tissue and one to laser resect tissue).

We utilized a TruLase Prostate HoLEP simulator (TPR100, TruCorp Ltd), which is designed for training surgeons in HoLEP (see Figure 16). This anatomically accurate simulator enables laser enucleation of a synthetic prostate specimen in a fluid-filled environment that mimics the conditions in clinical HoLEP surgery. The surgeon used both concentric tube manipulators in task space control, with a 500 μm holmium laser fiber passed through one manipulator, and the other used for tissue retraction. Both manipulators were identical two-tube, three-DOF devices, as shown in Figure 9.

The simulator was filled with saline solution and endoscopic saline irrigation was used in the same manner as in a clinical HoLEP procedure. The synthetic prostate used in this experiment was the three lobe prostate insert (TPRO-03, TruCorp Ltd) as shown in Figure 16. A clinical 80 W holmium laser was used, and the surgeon could fire the laser on demand using a foot pedal, just as they would in a clinical HoLEP case. The counterbalance arm was used and the endoscope (and robot) were free to be spatially oriented as desired. Two surgeons were asked to laser resect and remove a single lobe of the prostate and push it into the bladder, just as they would in a clinical HoLEP case (the specimen then gets morcellated within the bladder in the current clinical HoLEP procedure, and our system is designed to follow the same protocol for specimen removal). There were no restrictions or instructions regarding use of robotic manipulators versus endoscope pose control; surgeons were free to use both as they wished. Qualitatively we noticed that surgeons manipulated both endoscope pose and concentric tube manipulators simultaneously during the procedure and were not relying primarily on endoscope pose manipulation. It is also worth noting that this was each surgeon's first experience using both manipulators simultaneously.

Two lobes were successfully laser resected from the prostate model and pushed into the bladder, one by each surgeon. One surgeon removed the median lobe (the lobe in the center of Figure 16), while the other removed one of the lateral lobes. The post-experiment synthetic prostate model can be seen in Figure 17. After a short learning curve in which the surgeons focused primarily on the laser

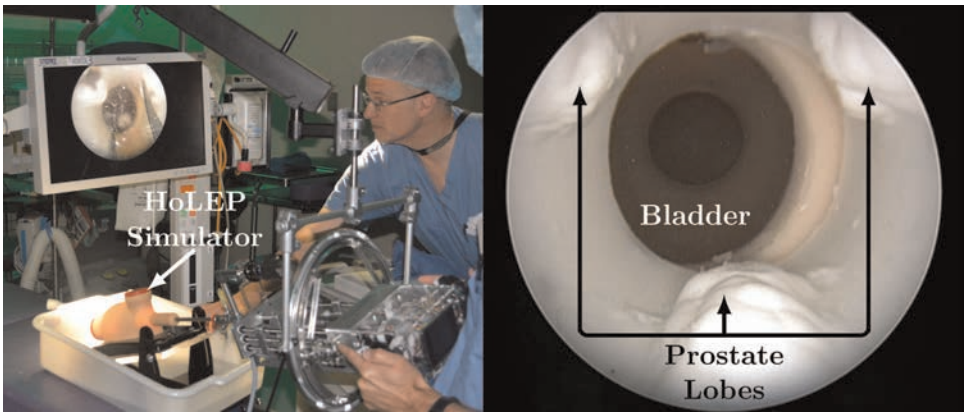

Fig. 16. (Left) The counterbalanced robot operates transurethrally through the HoLEP simulator. The surgeons visually servo the concentric tube manipulator tips in the task space with high-definition endoscopic video feedback. In this experiment, surgeons preferred a large off-board monitor to the onboard screen between their hands, though it is possible to show the endoscope image on either or both displays. (Right) The endoscopic view shows the three lobes of the synthetic prostate. Each surgeon was tasked with laser resecting one lobe of the prostate phantom.

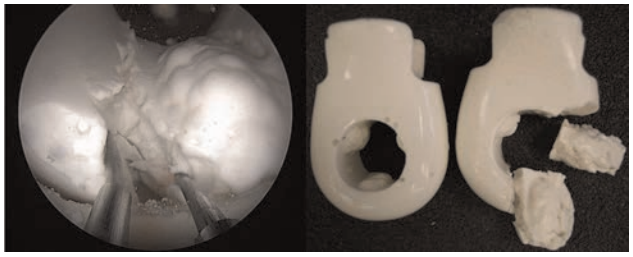

Fig. 17. (Left) The left manipulator retracts the tissue, exposing the targets for the right manipulator to cut with the holmium laser. (Right) A photograph of what the prostate model looked like before and after the experiment.

arm, surgeons began to use coordinated movement of both arms, increasingly relying on retraction from the retraction arm. The retraction arm was used to expose desired targets within tissue and the laser arm to cut the exposed surface with the laser.

4.4. Ex vivo laser resection of a cadaveric prostate specimen

To evaluate the system in biological tissues we used a dissected urethra, prostate, and bladder specimen for a lobe removal experiment similar to that conducted in phantoms in the previous section. The surgeon's goal in this experiment was to remove one of the lateral lobes of the prostate (the lateral lobes are considered more challenging to remove than the median lobe).

A challenge in this experiment was holding the specimen in a manner that approximates the surrounding tissue constraints present in the human body. To approximate these, we used sutures to loosely hold the specimen in place, with a layer of adhesive plastic wrap to provide a compliant support to the bladder, prostate, and urethra. To

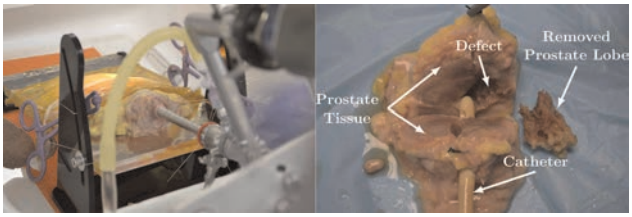

Fig. 18. (Left) The experimental setup shows the endoscope inserted into the specimen. The specimen is held with an adhesive plastic wrap and sutures through the specimen and the test stand. (Right) The dissected, sectioned post-operative specimen is shown. A catheter is placed through the urethra for reference, and the robotically removed 2.7 g lateral lobe is shown next to the specimen. The defect in the prostate where the lobe was removed is also visible.

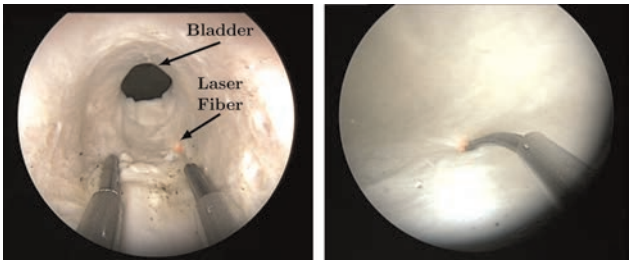

Fig. 19. (Left) An endoscopic view inside of the prostatic urethra shows both manipulators. (Right) The laser manipulator is shown endoscopically in the bladder.

perform the resection we again used the clinical 80 W holmium laser, which the surgeon could fire on demand using a foot pedal. Saline irrigation was provided through the endoscope, both manipulators were active, and the counterbalance was used. The experimental setup is shown in Figure 18 and two endoscopic views are shown in Figure 19.

The surgeon successfully removed a 2.7 g lateral lobe from the specimen (see Figure 18), using the robotic system for the entire procedure. The surgeon was able to resect the tissue up to the outside edge of the prostate (i.e. the prostate capsule) and enucleate the lobe, following the capsule around the organ during enucleation, mimicking the current surgical technique. The dissected and sectioned lobe of the prostate is shown postoperatively in Figure 18. We did note one small capsule perforation, indicating the need for further refinement and testing of the system, as well as perhaps the need for additional surgeon experience and training with the robot system (this was the surgeon's first cadaver case with the system). Future experiments are also needed to compare the robot to standard HoLEP in terms of procedure completion time, correspondence of actual enucleation volume to planned enucleation volume, and complication rates.

5. Conclusion

This paper has introduced a new system that enables hand-held coordination of both an endoscope and two concentric tube manipulators delivered through its 5 mm working channel. One useful feature of this robot is that it fits seamlessly into the clinical workflow of the HoLEP procedure in the sense that the surgeon maintains hand-held control of the endoscope and the patient and surgeon positions in the operating room are the same as in the current clinical workflow. We presented the mechanical design of the system and a method to select tube parameters in the concentric tube manipulator for optimal overlap of the manipulator's workspace and the endoscope's field of view. We also described the kinematics of the system and compared task and joint space control mappings via user studies with surgeons. This user study showed that the experimenting surgeons spent more time in large error states when utilizing joint space mode. Lastly, we described initial phantom and cadaver studies, which showed that the system can be used by surgeons to resect prostate lobes with the holmium laser. In the future, we plan to compare the system directly to the current manual approach in a series of user studies with experienced surgeons to explore our hypothesis that this robotic system has the potential to make HoLEP surgery easier to perform accurately and safely. If this hypothesis is proved correct, then the robot described in this paper may pave the way to wider use of the HoLEP procedure, and thereby enable many more patients to benefit from its demonstrated clinical benefits. We also believe that the basic concept behind our system, namely hand-held control of concentric tube robots extending through endoscopes, is generalizable to many other locations in the human body. Examples include endonasal surgery, throat surgery, brain surgery, and other surgeries that can benefit from dexterity in manipulators delivered through endoscopes. We believe that the hand-held paradigm is broadly applicable in surgical robotics, and user interfaces like the one we propose in this paper are a key to making them fit well enough into the existing workflow of the operating room that clinical personnel can easily adopt them.

Funding

This work was funded in part by the National Science Foundation (NSF) (IIS-105433 and Graduate Research Fellowship DGE-0909667) and in part by the National Institutes of Health (NIH) (R01 EB017467).

References

Abbott DJ, Becke C, Rothstein RI, et al. (2007) Design of an endoluminal notes robotic system. In: *IEEE/RSJ international conference on intelligent robots and systems*, pp. 410–416.

Ahyai SA, Lehrich K and Kuntz RM (2007) Holmium laser enucleation versus transurethral resection of the prostate: 3-year follow-up results of a randomized clinical trial. *European Urology* 52(5): 1456–1463.

Bedell C, Lock J, Gosline A, et al. (2011) Design optimization of concentric tube robots based on task and anatomical constraints. In: *IEEE international conference on robotics and automation*, pp. 398–403.

Burgner J, Gilbert HB and Webster RJIII (2013) On the computational design of concentric tube robots: Incorporating volume-based objectives. In: *IEEE international conference on robotics and automation*, pp. 1185–1190.

Burgner J, Rucker DC, Gilbert HB, et al. (2014) A telerobotic system for transnasal surgery. *IEEE/ASME Transactions on Mechatronics* 19(3): 996–1006.

Butler EJ, Hammond-Oakley R, Chawarski S, et al. (2012) Robotic neuro-endoscope with concentric tube augmentation. In: *IEEE/RSJ international conference on intelligent robots and systems*, pp. 2941–2946.

Camarillo DB, Krummel TM and Salisbury JKJr (2004) Robotic technology in surgery: Past, present, and future. *The American Journal of Surgery* 188(4): 2–15.

Chiaverini S (1997) Singularity-robust task-priority redundancy resolution for real-time kinematic control of robot manipulators. *IEEE Transactions on Robotics and Automation* 13(3): 398–410.

Davies B (2006) Medical robotics – a bright future. *Lancet* 368: S53–S54.

Davies BL, Hibberd RD, Ng WS, et al. (1991) The development of a surgeon robot for prostatectomies. *Proceedings of the Institution of Mechanical Engineers, Part H: Journal of Engineering in Medicine* 205: 35–38.

De Badajoz ES, Garrido AJ, Vacas FG, et al. (1998) New master arm for transurethral resection with a robot. *Archivos Espanoles de Urologia* 55: 1.247–1.250.

Ding J, Goldman RE, Xu K, et al. (2013) Design and coordination kinematics of an insertable robotic effectors platform for single-port access surgery. *IEEE/ASME Transactions on Mechatronics* 18(5): 1612–1624.

Dupont PE, Lock J, Itkowitz B, et al. (2010) Design and control of concentric-tube robots. *IEEE Transactions on Robotics* 26(2): 209–225.

Focacci F, Piccigallo M, Tonet O, et al. (2007) Lightweight hand-held robot for laparoscopic surgery. In: *IEEE international conference on robotics and automation*, pp. 599–604.

Goldman RE, Bajo A, MacLachlan LS, et al. (2013) Design and performance evaluation of a minimally invasive telerobotic platform for transurethral surveillance and intervention. *IEEE Transactions on Biomedical Engineering* 60(4): 918–925.

Hashimoto R, Kim D, Hata N, et al. (2004) A tubular organ resection manipulator for transurethral resection of the prostate. In: *IEEE/RSJ international conference on intelligent robots and systems*, pp. 3954–3959.

Hendrick RJ, Herrell SD and Webster RJIII (2014a) A multi-arm hand-held robotic system for transurethral laser prostate surgery. In: *IEEE international conference on robotics and automation*, pp. 2850–2855.

Hendrick RJ, Herrell SD, Mitchell CR, et al. (2014b) Experiments on the simultaneous hand-held control of rigid endoscopes and robots passing through them. In: *14th international symposium on experimental robotics*.

Hendrick RJ, Mitchell CR, Herrell SD, et al. (2014c) Concentric tube robots for transurethral prostate surgery: Matching the workspace to the endoscopic field of view. In: *The Hamlyn symposium on medical robotics*.

Ho G, Ng WS, Teo MY, et al. (2001) Experimental study of transurethral robotic laser resection of the prostate using the LaserTrode lightguide. *Journal of Biomedical Optics* 6(2): 244–251.

Leenstra JL, Davis BJ, Wilson TM, et al. (2007) Prostate dimensions and volume in 700 patients undergoing primary surgical or radiotherapeutic management of localized adenocarcinoma: Implications for design of minimally invasive prostate cancer devices. *International Journal of Radiation Oncology* 69(3): S380–S381.

Lehman AC, Wood NA, Farritor S, et al. (2011) Dexterous miniature robot for advanced minimally invasive surgery. *Surgical Endoscopy* 25(1): 119–123.

Lingeman JE (2011) Holmium laser enucleation of the prostate-if not now, when? *The Journal of Urology* 186(5): 1762–1763.

Mandeville J, Gnessin E and Lingeman JE (2011) New advances in benign prostatic hyperplasia: Laser therapy. *Current Urology Reports* 12(1): 56–61.

Murray RM, Li Z and Sastry SS (1994) *A Mathematical Introduction to Robotic Manipulation*. Boca Raton, FL: CRC Press.

Okazawa S, Ebrahimi R, Chuang J, et al. (2005) Hand-held steerable needle device. *IEEE/ASME Transactions on Mechatronics* 10(3): 285–296.

Phee SJ, Low SC, Sun ZL, et al. (2008) Robotic system for no-scar gastrointestinal surgery. *The International Journal of Medical Robotics and Computer Assisted Surgery* 4(1): 15–22.

Piccigallo M, Scarfogliero U, Quaglia C, et al. (2010) Design of a novel bimanual robotic system for single-port laparoscopy. *IEEE/ASME Transactions on Mechatronics* 15(6): 871–878.

Rodriguez y, Baena F and Davies B (2010) Robotic surgery: From autonomous systems to intelligent tools. *Robotica* 28: 163–170.

Rucker DC, Jones BA and Webster RJ III (2010) A geometrically exact model for externally loaded concentric-tube continuum robots. *IEEE Transactions on Robotics* 26(5): 769–780.

Sears P and Dupont P (2006) A steerable needle technology using curved concentric tubes. In: *IEEE/RSJ international conference on intelligent robots and systems*, pp. 2850–2856.

Shang J, Noonan DP, Payne C, et al. (2011) An articulated universal joint based flexible access robot for minimally invasive surgery. In: *IEEE international conference on robotics and automation*, pp. 1147–1152.

Shang J, Payne CJ, Clark J, et al. (2012) Design of a multitasking robotic platform with flexible arms and articulated head for minimally invasive surgery. In: *IEEE/RSJ international conference on intelligent robots and systems*, pp. 1988–1993.

Swanstrom L and Zheng B (2008) Spatial orientation and off-axis challenges for notes. *Gastrointestinal Endoscopy Clinics of North America* 18(2): 315–324.

Taylor RH and Stoianovici D (2003) Medical robotics in computer-integrated surgery. *IEEE Transactions on Robotics and Automation* 19(5): 765–781.

Van Rij S and Gilling PJ (2012) In 2013, holmium laser enucleation of the prostate (HoLEP) may be the new 'gold standard'. *Current Urology Reports* 13: 427–432.

Wampler CW II (1986) Manipulator inverse kinematic solutions based on vector formulations and damped least-squares methods. *IEEE Transactions on Systems, Man, and Cybernetics* 16(1): 93–101.

Webster RJ III and Jones BA (2010) Design and kinematic modeling of constant curvature continuum robots: A review. *The International Journal of Robotics Research* 29(13): 1661–1683.

Webster RJ III, Okamura A and Cowan NJ (2006) Toward active cannulas: Miniature snake-like surgical robots. In: *IEEE/RSJ international conference on intelligent robots and systems*, pp. 2857–2863.

Wei W, Goldman RE, Fine HF, et al. (2009) Performance evaluation for multi-arm manipulation of hollow suspended organs. *IEEE Transactions on Robotics* 25(1): 147–157.

Xu R and Patel RV (2012) A fast torsionally compliant kinematic model of concentric-tube robots. In: *Annual international conference of the IEEE Engineering in Medicine and Biology Society*, pp. 904–907.

Yamashita H, Hata N, Hashizume M, et al. (2004) Handheld laparoscopic forceps manipulator using multi-slider linkage mechanisms. *Medical Image Computing and Computer-Assisted Intervention* 3217: 121–128.